Journal of Materials Chemistry B

PAPER

View Article Online
View Journal | View Issue

A rheumatoid arthritis magnetic resonance imaging contrast agent based on folic acid conjugated PEG-*b*-PAA@SPION†

Cite this: *J. Mater. Chem. B*, 2014, **2**, 2938

Yanqi Zhong,‡[ab] Fengying Dai,‡[a] Heng Deng,[ab] Meihong Du,[c] Xiaoning Zhang,*[d] Qingjun Liu*[c] and Xin Zhang*[a]

Received 14th January 2014
Accepted 20th February 2014

DOI: 10.1039/c4tb00085d

www.rsc.org/MaterialsB

Superparamagnetic iron oxide nanoparticles (SPIONs) offer unique properties for magnetic resonance imaging (MRI). Targeting imaging of rheumatoid arthritis *in vivo* requires a specific, magnetic sensitive and ultra-stable MRI contrast agent. In this study, SPIONs with a preferable colloid stability and optimized size were obtained by using an *in situ* polyol method with the diblock copolymer PEG-*b*-PAA acting as a surface ligand. Increasing the degree of polymerization (DP) of PAA from 18 to 36 to 57 led to the decreasing size of the iron oxide nanoparticles from 52 nm to 17 nm to 9 nm, respectively. Folic acid was conjugated onto PEG-PAA$_x$@SPION as a specific targeting molecule for activated macrophages in a rheumatoid arthritis joint. To evaluate the stability and magnetic properties of the particle, a series of tests were conducted to evaluate and optimize the nanoparticles. *In vitro* endocytosis experiments confirmed the better performance of the folic acid conjugated SPIONs than the non-folic acid modified SPIONs. *In vivo* MRI clearly demonstrated the significant signal diminishment of the arthritis joint in antigen induced arthritis (AIA) rats by intravenous injection of the optimized nanoparticles FA–PEG-*b*-PAA$_{36}$@SPION. These results indicated that FA–PEG-*b*-PAA$_{36}$@SPION could serve as a promising candidate for the MRI of rheumatoid arthritis.

1 Introduction

Rheumatoid arthritis (RA) is a permanent and incurable disease which causes a high degree of morbidity.[1] Therefore, diagnosing the disease and assessing its severity is crucial for preventing the exacerbation of the disease. Among the clinical imaging methods, magnetic resonance imaging (MRI) harbors a number of advantages including a high spatial resolution and soft-tissue resolution over conventional radiography, which enable the characterization of the structural damage of the joint in unprecedented detail and depth.[2] However, as one of the most commonly used T_1 weighted MR contrast agents, gadopentetate dimeglumine (Magnevist) shows some limitations in distinguishing between a normal and arthritic joint and fails to faithfully recapitulate all the facets of the arthritic joints including the degree of inflammatory cell recruitment.[3]

SPION contrast agents can pass through the microvascular system, be endocytosed by macrophages and serve as molecule imaging agents to contrast and characterize the structure of the joint.[3] In the past few years, many researchers have focused on using SPIONs as MRI contrast agents for RA imaging.[4,5] Hydrophobic nanoparticles produced by high-temperature thermo-decomposition reactions possess excellent magnetic sensitivities. However, hydrophobic nanoparticles need further modifications to transfer into the water phase, which may lead to them being physiological unstable or aggregating.[6–8] Moreover, controlling the core size of the nanoparticles is indispensable since larger nanoparticles may be endocytosed by the RES system, whereas smaller nanoparticles suffer from weak magnetic sensitivities. Finally, without active-targeting molecules, SPIONs have shown a limited MR signal enhancement.[8–10] Centering on these problems, this paper puts forward an *in situ* polyol synthesized PEG-*b*-PAA@SPION contrast by a thermo-decomposition reaction with a high crystallinity and MR sensitivity. A PEG coating was incorporated to offer a good colloidal stability for the magnetic iron oxide particles and a proper length PAA block was used to control the core size of the nanoparticles.[11–13] Folic acid was conjugated onto PEG-*b*-PAA@SPION for its target binding to recruit and activate macrophages in the synovium.[14] To reach a balance between the

[a]*National Key Laboratory of Biochemical Engineering, Institute of Process Engineering, Chinese Academy of Sciences, Beijing, 100190, PR China. E-mail: xzhang@home.ipe.ac.cn; Fax: +86 010 82544853; Tel: +86 010 82544853*

[b]*University of Chinese Academy of Sciences, Beijing, 100049, PR China*

[c]*Beijing Center for Physical and Chemical Analysis, Beijing, 100089, PR China. E-mail: Liuqj@bjast.ac.cn; Tel: +86 010 88487669*

[d]*School of Medicine, Tsinghua University, Beijing, 100084, China. E-mail: drugman@mail.tsinghua.edu.cn; Fax: +86 010 62785410; Tel: +86 010 62785489*

† Electronic supplementary information (ESI) available. See DOI: 10.1039/c4tb00085d

‡ Yanqi Zhong and Fengying Dai contributed equally to this work.

stability and the magnetic properties of the particle, we have specifically designed a series of SPIONs with different core sizes. Various tests were conducted to evaluate and optimize the nanoparticles. With the selected nanoparticle PEG-*b*-PAA@SPION, the MRI experiment exhibited an enhanced performance in the diagnosis of RA *in vivo*.

2 Experimental section

2.1 Materials

HO–PEG–OH ($M_w = 2000$), iron(III) acetylacetonate ($Fe(acca)_3$), *tert*-butyl acrylate, folic acid (FA), dicyclohexylcarbodiimide (DCC), 4-dimethylamiopyridine (DMAP), triethylene glycol (TREG) and trifluoroacetic acid (TFA) were purchased from Aladdin Reagent (Shanghai, China). 2-Bromoisobutyryl bromide (98%), copper bromide (CuBr, 98%), *N*,*N*,*N*′,*N*′,*N*″-pentamethyldiethylenetriamine (PMDETA, 99%) and triethylamine (TEA, ≥99%) were purchased from Sigma-Aldrich (St. Louis, Missouri). All the reagents were of analytical grade and used without further purification. High-purity water (Milli-Q Integral) with a conductivity of 18 MΩ cm^{-1} was used for the preparation of all aqueous solutions.

2.2 The synthesis of HO–PEG–Br

PEG-*b*-PAA_x diblock copolymers were synthesized by atom transfer radical polymerization (ATRP). Macroinitiator HO–PEG–Br was first synthesized by the reaction of HO–PEG–OH and 2-bromoisobutyryl bromide.[15] In brief, 10 g HO–PEG–OH and 0.505 g triethylamine were dissolved in 20 mL anhydrous dichloromethane, and then 1.15 g 2-bromoisobutyryl bromide dissolved in anhydrous dichloromethane was added dropwise with gentle stirring at 0 °C. The solution was warmed to room temperature and stirred for 48 h. The mixture was washed three times with the saturated sodium chloride solution containing a few drops of concentrated hydrochloric acid and then precipitated in cold diethyl ether.

2.3 The synthesis of PEG-PAA_x

HO–PEG–Br (1 equiv.) was dissolved in a mixed solvent of 2-butanone and isopropanol (7 : 3), and then PMDETA (1.1 equiv.), Cu(I)Br (1.1 equiv.) and the monomers (5–100 equiv.) were added. The mixture was degassed with nitrogen for 30 minutes and reacted at 50 °C for 24 hours. By controlling the different ratios of the *t*BA monomer and the macroinitiator HO–PEG–Br, PEG-*b*-PAA_x with different *t*BA chain lengths were obtained. Specifically, PEG-*b*-P*t*BA_{57}, PEG-*b*-P*t*BA_{36} and PEG-*b*-P*t*BA_{18} were polymerized by the initiator/monomer ratios of 100 : 1, 60 : 1 and 30 : 1, respectively. The mixture was filtered through an alumina column to remove copper and was dialyzed against deionized water to remove the residual *t*BA monomer and then lyophilized to obtain a white powder. The obtained PEG-*b*-PAA_x was hydrolyzed in the solution of trifluoroacetic acid and dichloromethane (1 : 1) for 24 h. Residual TFA and dichloromethane were removed by rotary evaporation and a light yellow sticky product was obtained.

2.4 The synthesis of PEG-*b*-PAA_x@SPION

The synthesis was conducted as follows: 1.0 g PEG-*b*-PAA_x was dissolved in 25 mL triethylene glycol in 100 °C. 1.0 g $Fe(acac)_3$ was added after the polymer was completely dissolved. The mixture was heated to 190 °C for 30 minutes. Afterwards the solution was refluxed at 290 °C under a blanket of nitrogen for 30 minutes. The black product was then dialyzed against deionized water for 2 days and separated *via* centrifugation of 15 000 rpm.

2.5 The conjugation of folic acid

The conjugation of folic acid was achieved *via* a DCC/DMAP reaction. Folic acid (1 equiv.) and DCC (1 equiv.) were add to anhydrous DMSO and stirred overnight. PEG-PAA@SPION (1 equiv. of HO-PEG-PAA_x) and DMAP (0.1 equiv.) were then added. The solution was stirred for 24 h and the nanoparticles were separated *via* centrifugation of 15 000 rpm.

2.6 The stability of PEG-PAA_x@SPION and FA–PEG-PAA_x@SPION

The stability test of PEG-*b*-PAA_x@SPION and FA–PEG-*b*-PAA_x@SPION was conducted by measuring the hydrodynamic diameter of the nanoparticles dispersed into DMEM cell culture medium (10% FBS) for different periods of time (0, 12, 24, 48 and 72 hours). The hydrodynamic diameter was measured by dynamic light scattering (DLS) following a previous report.[16] Triple measurements of the number-weighted mean size were performed.

2.7 Characterizations

The structure of PEG-*b*-PAA_x was examined by NMR (Bruker Avance 600 MHz, Bruker AXS Inc., Madison, Wisconsin). The hydrodynamic size and size distribution of the particles were measured by dynamic light scattering using a Malvern Zetasizer nano ZS apparatus (Malvern Instruments, Malvern, United Kingdom). The morphology of PEG-*b*-PAA_x@SPION was observed by transmission electron microscopy (TEM, JEOL 2100F) at 120 kV. Thermogravimetric analysis (TGA) was performed using a TG-209-F3 thermogravimetric analyzer (Netzsch Instruments, Germany) with a heating rate of 10 °C min^{-1} from 30 to 800 °C in an N_2 atmosphere. Magnetic measurements were carried out at room temperature using a MPMS XL-7 Quantum Design SQUID magnetometer (Quantum Design, America, San Diego) with the H magnetic intensity ranging from -1×10^4 to 1×10^4. UV vis spectrophotometry measurements were performed on a TU-1810 ultraviolet and visible spectrophotometer (Persee, China) with a wavelength range from 250 nm to 800 nm. The surface compositions of the nanoparticles were analyzed *via* X-ray photoelectron spectroscopy (XPS) on a Thermo Escalab 250Xi (Thermo, America) with a monochromatized Al Kα X-ray source. The samples were mounted on the standard sample studs using double-sided adhesive tapes. The reference for the binding energies (BEs) was 284.8 eV (C 1s hydrocarbon peak). The NMR relaxometry of PEG-*b*-PAA_x@SPION was measured by a NMR spectrometer (Minispec, mq60,

Bruker, Germany). The nanoparticles were dispersed in water with iron concentrations from 0.01 to 10 mM. The Carr–Purcell–Meiboom–Gill pulse sequence was used to measure T_2 relaxation time, and the slope of linear fit of $1/T_2$ *versus* iron concentrations is the r_2 value of the SPIONs.

2.8 Cell culture and Prussian blue staining of cells

RAW 264.7 cells were purchased from Fuxiang biotech company, China, Shanghai. The cells were cultured in 12-well polystyrene dishes at 37 °C in a humidified atmosphere of 5% CO_2 and 95% air in DMEM high glucose medium containing 10% FBS and supplemented with penicillin (100 units per mL) and streptomycin (100 units per mL). The activation of the RAW 264.7 cells was conducted as described previously.[17] RAW 264.7 cells were plated in a 24-well plate at density of 2×10^4 per well, and cytokines IFN-γ and TNF-α were added to the cell culture medium with the final concentration of 200 U mL^{-1} and 100 U mL^{-1} for 24 hours. The concentration and time dependent RAW 264.7 cell uptake of FA–PEG-*b*-PAA_x@SPION were conducted by co-culturing SPION with the RAW 264.7 cells at different times or concentrations. Once the incubation was ended, the cells were washed with PBS three times, fixed with 500 μL paraformaldehyde (4%) for 30 minutes, and then incubated for 30 minutes at 37 °C with a 500 μL Prussian blue solution containing 10% hydrochloride and 20% potassium ferrocyanide(II) trihydrate.

2.9 Ferrozine assay

The iron concentrations were measured using the ferrozine assay. The cells were washed three times with PBS after incubation. 250 μL reagent A (4.5% $KMnO_4$ and 1.2 M HCl mixed at equal volumes) was added and mixed for 1 hour. After that 50 μL reagent B (6.5 mM ferrozine, 13.1 mM neocuproine, 2 M ascorbic acid and 5 M ammonium acetate) was added. The absorbance of the samples was tested at 570 nm using a Bio-Radmicroplate reader and the standard curve was prepared with ferrous ethylenediammonium sulphate in 0.01 M HCl, ranging from 0 to 60 mg mL^{-1}.

2.10 The SPION enhanced MRI of antigen-induced arthritis

All procedures involving experimental animals were performed in accordance with the Guide for the Care and Use of Laboratory Animals (NIH publication no. 86-23, revised 1985). Lewis rats were sensitized by an intradermal injection in the back feet with 100 μL complete Freund's adjuvant mixed and completely emulsified with physiological saline. Joint inflammation was assessed by measuring the diameter of the ankle joint. The inflammation of the four paws was graded from 0 to 4 according to previous literature.[18] After 14 days, the animals were all graded to validate the AIA model for further use. 21 days after the injection with complete Freund's adjuvant, the animals were intravenous injected with PEG-*b*-PAA_{36}@SPION or FA–PEG-*b*-PAA_{36}@SPION at a dose of 5 mg kg^{-1}. The infected right hind ankle was imaged with a 7-T Bruker (Bruker Medical Systems, Germany). The T_2-weighted imaging sequence was applied and a transverse section orientation was selected. The signal intensity was quantified through the signal intensity ratio of the surrounding water proton/the arrowhead indicated area. The parameters were as follows: TR = 3000, TE = 45, matrix = 256 × 256, field of view (FOV) = 3.0 × 3.0 cm^2, slice thickness = 1.00 mm and the number of excitation (NEX) = 1.

2.11 Histopathology assessment

After the MRI, the animals were sacrificed. The main organs and ankle joints were harvested and fixed in 10% neutral buffered formalin for 24 hours. After that they were decalcified over night, and processed through a gradient of alcohols for paraffin embedding. For hematoxylin–eosin staining, the slides were immersed in the stain, washed, and mounted in *p*-xylene-bis-pyridiniumbromide (VWR, Dorset, England) with obtained tissue section of 5 μm. For Prussian blue staining, the slides were incubated with an equal mixture of fresh 2% hydrochloric acid and 2% potassium ferrocyanide for 30 minutes at room temperature. Afterwards, the slides were washed and counter-stained with nuclear fast red.

3 Results and discussion

3.1 The preparation and characterization of PEG-*b*-PAA_x@SPION

The synthesis of the magnetite nanoparticles was carried out by reacting the iron precursor, iron(III) acetylacetonate ($Fe(acac)_3$), with PEG-*b*-PAA_x at an elevated temperature. The block copolymer of PEG-*b*-PAA_x in this reaction played a dual role in controlling the core size of the iron oxide particles efficiently and enhancing the colloidal stability of the iron oxide particles in the physiological environment. Learning from the previous studies that an exceedingly long chain of PEG might have an adverse impact on the r_2 relaxation, a moderate length of PEG ($M_w = 2000$) was adopted in our study.[19,20] Three block copolymers of PEG-*b*-PAA_x with different chain lengths of PAA were synthesized *via* ATRP. The synthesis route for the PEG-*b*-PAA_x coated SPIONs is shown in Scheme 1.

Fig. 1 shows the ^{1}H NMR spectra of the HO–PEG–Br, PEG-*b*-P*t*BA_x and PEG-*b*-PAA_x block polymer. In the macroinitiator HO–PEG–Br, feature signals of –CH_2–CH_2O– ($\delta = 3.68$) and –$C(CH_3)_2$Br ($\delta = 1.98$) appeared, which indicated the formation of OH–PEG–Br. The structure of PEG-*b*-P*t*BA_x was confirmed by the feature peaks of –$C(CH_3)_3$ ($\delta = 1.45$), –C*H*–CH_2– ($\delta = 2.23$) and –CH–CH_2– ($\delta = 1.86$), which belonged to the P*t*BA block. After the copolymers were hydrolyzed by trifluoroacetic acid (TFA), the peak of –$C(CH_3)_3$ disappeared and the two peaks of the main chain –C*H*–CH_2– ($\delta = 2.31$) and –CH–CH_2– ($\delta = 1.51$) were slightly moved.[21,22] The DP (degree of polymerization) was calculated according to the integral area ratio. For instance, the DP of P*t*BA was calculated to be 36 based on the integral area ratio of –CH_2–CH_2O– and –$C(CH_3)_3$, Fig. S1† shows the ^{1}H NMR spectra of the three kinds of PEG-*b*-P*t*BA_x. The DP of P*t*BA could be calculated from the integral area ratio of –CH_2–CH_2O– and –$C(CH_3)_3$. By controlling the amount of the *t*BA monomer added, PEG-*b*-P*t*BA_{18}, PEG-*b*-P*t*BA_{36} and PEG-*b*-P*t*BA_{57} were synthesized.[23,24]

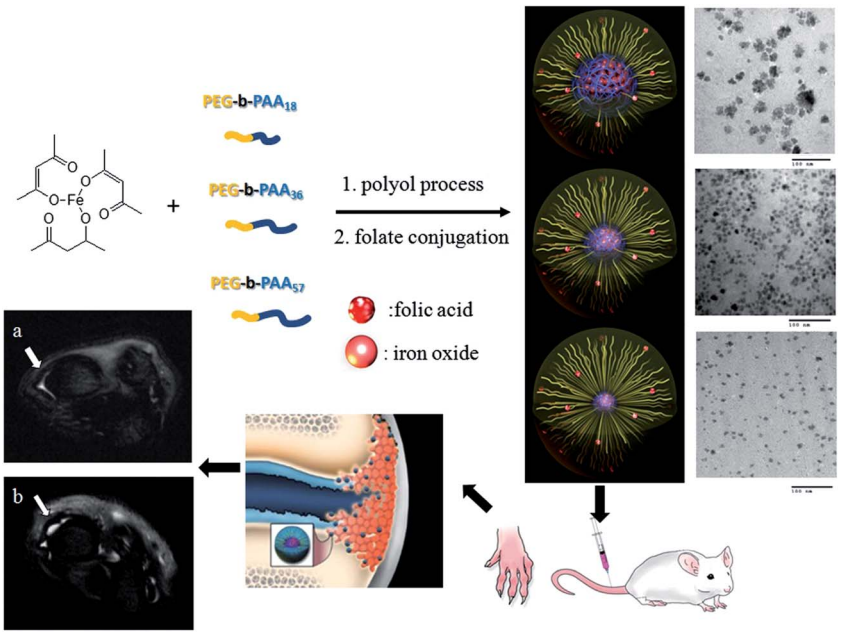

Scheme 1 A schematic representation of the PEG-*b*-PAA$_x$@SPION synthesis with different core sizes and an evaluation of the optimized nanoparticles for enhanced magnetic resonance imaging of rheumatoid arthritis. The iron oxide cores are imaged to be red small balls in the scheme. The PEG chains (yellow colored lines) are coated on the outer shell of the nanoparticle while the PAA chains (blue colored lines) are firmly attached to the surface of the core. The folic acid molecules are represented as red small balls which are conjugated on the end of the PEG molecules.

3.2 The size and colloid stability of PEG-PAA$_x$@SPION

The size of the iron oxide nanoparticles was confirmed by transmission electron microscopy and dynamic light scattering analysis in aqueous medium (Fig. 2 and Table 1). The TEM observation result indicated that PEG-*b*-PAA$_{57}$@SPION and PEG-*b*-PAA$_{36}$@SPION presented similar mono-dispersed and spherical-like structures. The average core sizes of these two particles were 6.6 ± 0.7 nm and 12.4 ± 1.3 nm, respectively,

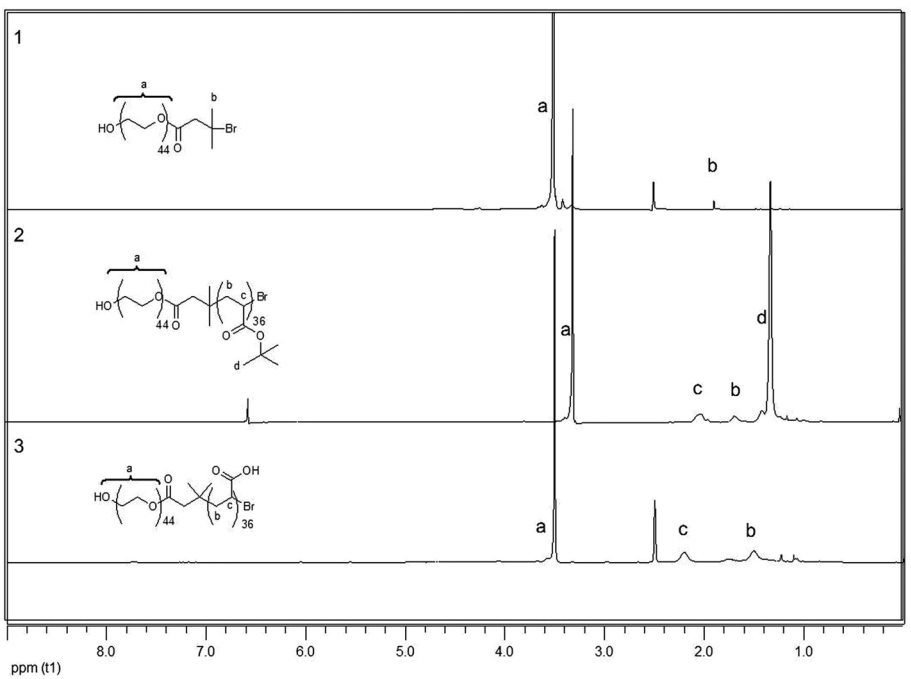

Fig. 1 The ^{1}H NMR spectra of (1) HO-PEG-Br dissolved in DMSO-d6; (2) PEG-*b*-P*t*BA$_{36}$ dissolved in $CDCl_3$ and (3) PEG-*b*-PAA$_{36}$ dissolved in DMSO-d6.

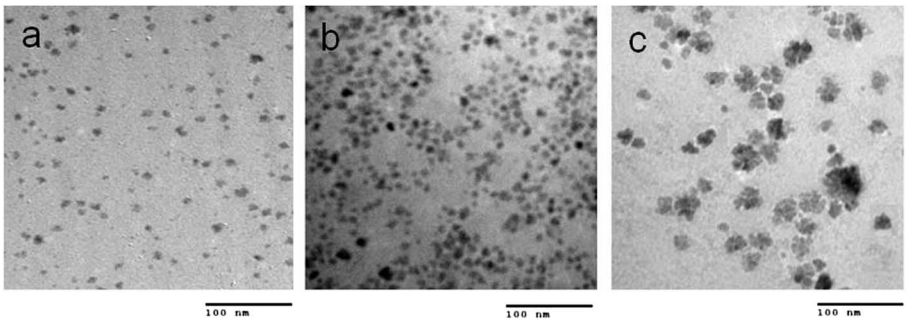

Fig. 2 The TEM images of (a) PEG-*b*-PAA_{57}@SPION; (b) PEG-*b*-PAA_{36}@SPION and (c) PEG-*b*-PAA_{18}@SPION.

Table 1 The hydrodynamic size and core size of PEG-*b*-PAA_{57}@SPION, PEG-*b*-PAA_{36}@SPION and PEG-*b*-PAA_{18}@SPION

Polymer coated nanoparticles	Core size (nm)	Hydrodynamic size (nm)
PEG-*b*-PAA_{57}@SPION	6.6 ± 0.7	9.2 ± 1.2
PEG-*b*-PAA_{36}@SPION	12.4 ± 1.3	17.7 ± 1.4
PEG-*b*-PAA_{18}@SPION	36.6 ± 9.3	52.0 ± 5.2

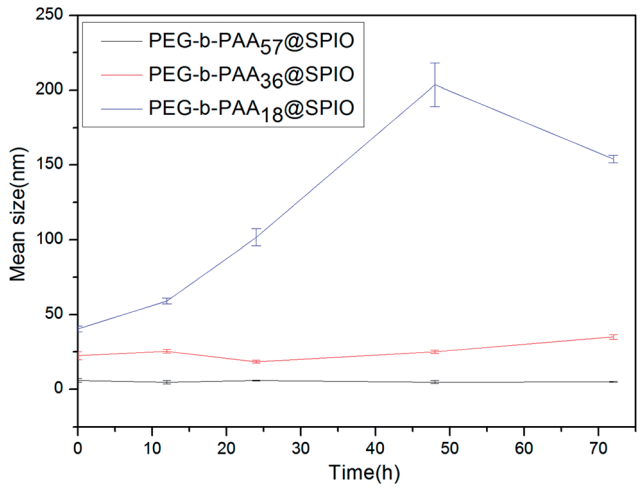

Fig. 3 The serum stability of PEG-*b*-PAA_x@SPION.

whereas PEG-*b*-PAA_{18}@SPION showed a larger core size of 36.6 ± 9.3 nm. This might result from the inefficiency in controlling the iron oxide crystal growth of the shorter chain length of PAA_{18} and the structure of PEG-*b*-PAA_{18}@SPION was largely consistent with a recent report on the polyol process synthesis of iron oxide nanoparticles.[25] The hydrodynamic diameters of PEG-*b*-PAA_{57}@SPION, PEG-*b*-PAA_{36}@SPION and PEG-*b*-PAA_{18}@SPION were 9.2 ± 1.2 nm, 17.7 ± 1.4 nm and 52.0 ± 5.2 nm, respectively, which are consistent with the TEM results (Table 1).

The colloid stability was very important for the design of the SPIONs as MRI contrast agents. To assess the stability of the SPIONs, the nanoparticles were incubated in DMEM cell culture medium containing 10% FBS and the hydrodynamic sizes were tested by DLS at different times (Fig. 3). PEG-*b*-PAA_{36}@SPION and PEG-*b*-PAA_{57}@SPION were stable and did not have any significant change for 72 hours, whereas PEG-*b*-PAA_{18}@SPION tended to aggregate and gradually precipitate in the solution. The optimized magnetic particles PEG-*b*-PAA_{36}@SPION and PEG-*b*-PAA_{57}@SPION were selected for further arthritis MRI study.

3.3 The synthesis of the folic acid conjugated PEG-PAA_x@SPION

Macrophages play a major role in various stages of RA, as previous research has shown that the MRI signal of normal synovium remained constant after the intravenous administration of SPIONs since there were no activated macrophages in the normal synovium.[26] Macrophages have been proven to be a biomarker for the inflamed lesions assessment of RA. SPION MRI contrast agent targeting macrophages might have a high sensitivity and specificity for the evaluation of RA. In this section, folic acid conjugated PEG-PAA_x@SPION for targeting MRI of rheumatoid arthritis was obtained by an esterification reaction. The conjugation of folic acid and SPION was confirmed by XPS as seen in Fig. 4a and b. The N1s peak was shown in the wild-scan spectra of FA–PEG-*b*-PAA_{57}@SPION and FA–PEG-*b*-PAA_{36}@SPION, whereas no significant N1s peaks were found in the spectra of PEG-*b*-PAA_{57}@SPION and PEG-*b*-PAA_{36}@SPION. The C1s core-level spectra of PEG-*b*-PAA_{57}@SPION and PEG-*b*-PAA_{36}@SPION (Fig. 4c and d) could both be curve-fitted with three peaks at the binding energies (BEs) of 284.6, 286.2 and 288.6 eV, which were attributed to the C–C/C–H, C–O, and O=C–O bonds, respectively.[27] In comparison, two new peaks at 285.6 and 287.8 eV in FA–PEG-*b*-PAA_{57}@SPION and FA–PEG-*b*-PAA_{36}@SPION (Fig. 4e and f) were attributed to the peaks of the C–N and O=C–N bonds, which belong to the conjugated folic acid.[28] A UV spectrophotometry method (Fig. 5) was also used to verify the existence of folic acid. The characteristic absorption peak of folic acid located at 280 nm was exhibited in the spectra of FA–PEG-*b*-PAA_{57}@SPION and FA–PEG-*b*-PAA_{36}@SPION,[29] while it was absent in the spectra of PEG-*b*-PAA_{57}@SPION and PEG-*b*-PAA_{36}@SPION. The UV-vis spectrophotometry feature of the folic acid conjugated SPIONs was consistent with a previous report on the chemical conjugation of FA.[30] The conjugation of FA onto the particles could be quantified by using a calibration curve of free FA (Fig. S3†). The amount of the conjugated FA was calculated to be 40.7 and 20.5

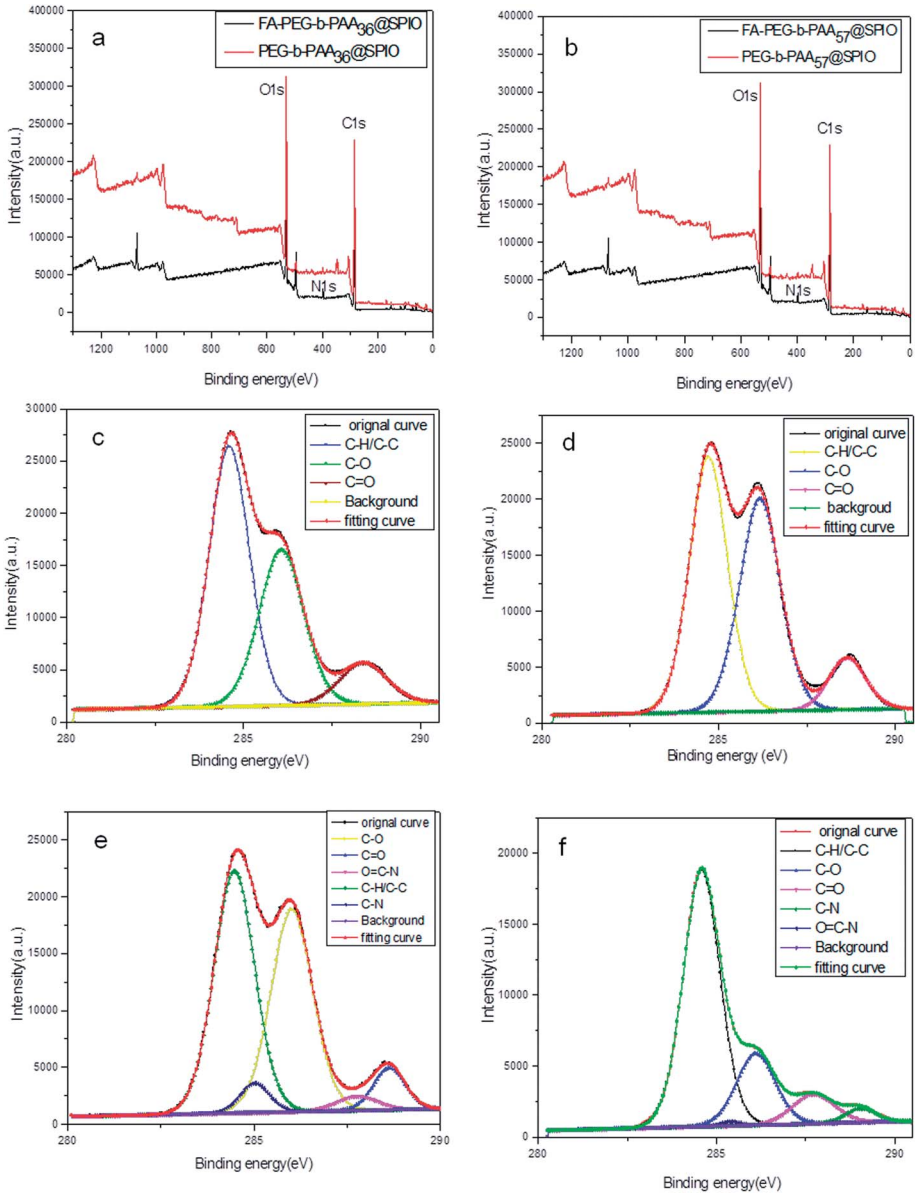

Fig. 4 The XPS wild scan spectra of FA–PEG-*b*-PAA_{36}@SPION and FA–PEG-*b*-PAA_{57}@SPION (a and b); the C1s core-level spectra of PEG-*b*-PAA_{36}@SPION (c); the C1s core-level spectra of FA-PEG-*b*-PAA_{36}@SPION (e); the C1s core-level spectra of PEG-*b*-PAA_{57}@SPION (d); the C1s core-level spectra of FA-PEG-*b*-PAA_{57}@SPION (f).

mg per g per nanoparticles for FA–PEG-*b*-PAA_{36}@SPION and FA–PEG-*b*-PAA_{57}, respectively.

3.4 The magnetic properties of PEG-PAA_x@SPION and FA–PEG-PAA_x@SPION

Hysteresis loops measured by a vibrating sample magnetometer exhibited similar superparamagnetic characteristics with no remnant magnetization and coercivity of PEG-*b*-PAA_{36}@SPION and PEG-*b*-PAA_{57}@SPION as well as folic acid conjugated FA–PEG-*b*-PAA_{36}@SPION and FA–PEG-*b*-PAA_{57}@SPION at room temperature (Fig. 6). Based on the TGA results (Fig. S2†), the saturation magnetizations (M_s) of PEG-*b*-PAA_{36}@SPION and PEG-*b*-PAA_{57}@SPION were calculated to be 54.3 Fe emu g^{-1} and 17.0 Fe emu g^{-1}, respectively, and the M_s for FA–PEG-*b*-PAA_{36}@SPION and FA–PEG-*b*-PAA_{57}@SPION were 53.1 Fe emu g^{-1} and 13.7 Fe emu g^{-1}, respectively, which indicated no obvious loss of magnetization per Fe unit after the conjugation of folic acid.

To further assess their magnetic properties for MRI applications, the r_2 relaxivities of the nanoparticles were calculated by measuring the change of the spin–spin relaxation rate (T_2^{-1}) per unit Fe concentration. The r_2 of PEG-*b*-PAA_{36}@SPION and FA–PEG-*b*-PAA_{36}@SPION were significantly larger than those of PEG-*b*-PAA_{57}@SPION and FA–PEG-*b*-PAA_{57}@SPION, whereas the conjugation of folic acid possess little impact on the r_2 value of the nanoparticle. The hysteresis loops and r_2 relaxivity results indicated that PEG-*b*-PAA_{36}@SPION was much more magnetic

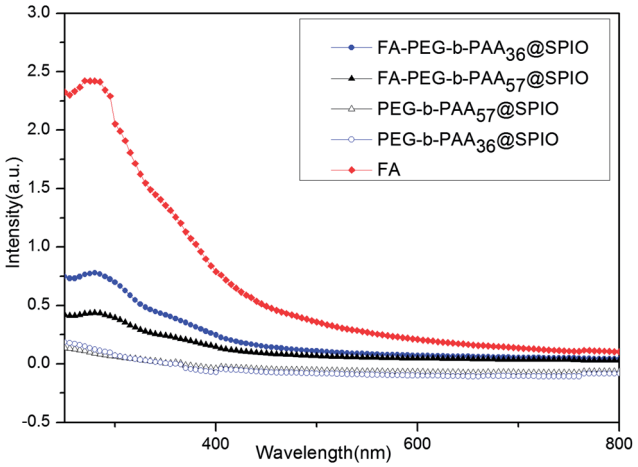

Fig. 5 The UV-vis absorption spectra of PEG-*b*-PAA$_{57}$@SPION, PEG-*b*-PAA$_{36}$@SPION, FA–PEG-*b*-PAA$_{36}$@SPION, FA–PEG-*b*-PAA$_{57}$@SPION and folic acid in DI water.

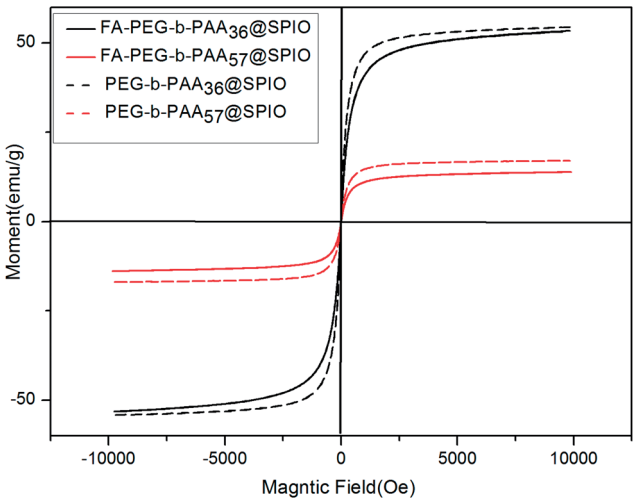

Fig. 6 The magnetization curves of PEG-*b*-PAA$_{36}$@SPION, FA–PEG-*b*-PAA$_{36}$@SPION, PEG-*b*-PAA$_{57}$@SPION and FA–PEG-*b*-PAA$_{57}$@SPION.

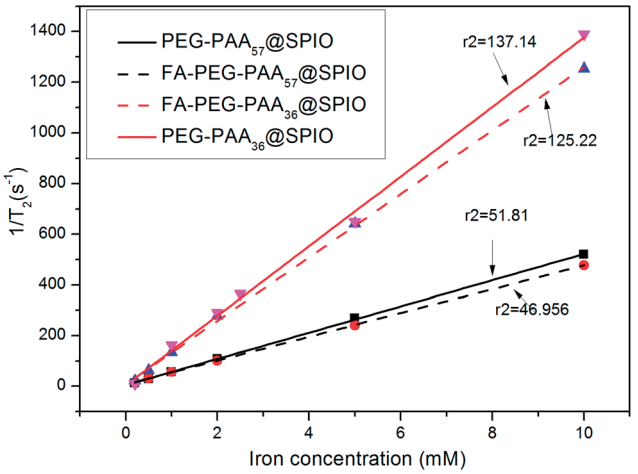

Fig. 7 A plot of r_2 as a function of the iron concentration of PEG-*b*-PAA$_{36}$@SPION, FA–PEG-*b*-PAA$_{36}$@SPION, PEG-*b*-PAA$_{57}$@SPION and FA–PEG-*b*-PAA$_{57}$@SPION.

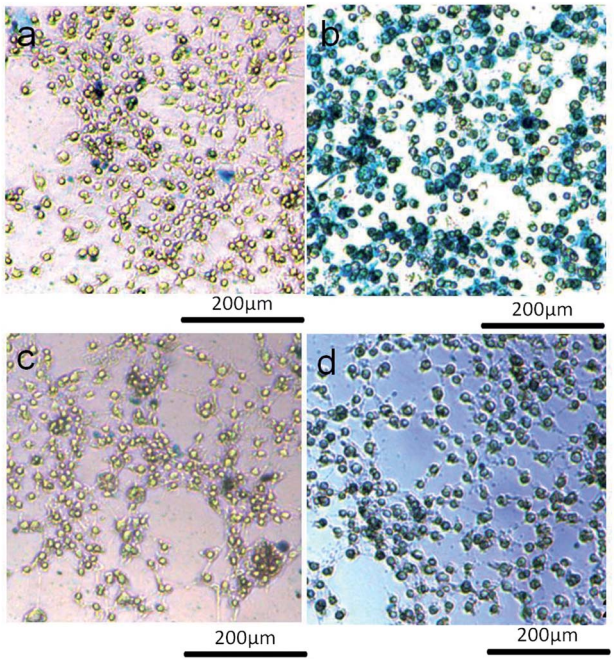

Fig. 8 The Prussia staining of the RAW 264.7 cell uptake of FA–PEG-*b*-PAA$_{57}$@SPION (a), FA–PEG-*b*-PAA$_{36}$@SPION (b), PEG-*b*-PAA$_{57}$@SPION (c), and PEG-*b*-PAA$_{36}$@SPION (d).

sensitive than PEG-*b*-PAA$_{57}$@SPION. This might be attributed to the larger core size and therefore the smaller spin canting effect of PEG-*b*-PAA$_{36}$@SPION.[31,32] The r_2 value of FA–PEG-*b*-PAA$_{36}$@SPION was close to that of Resovist,[31] a commercial SPION for lymph node imaging which has a hydrodynamic size of about 40 nm. The reason for the similarity might lie in the fact that commercial Resovist was obtained by the co-precipitation method, while the polyol method produced PEG-*b*-PAA@SPION were prepared under high temperature conditions. Due to the strong Ostwald ripening procedure, the crystallinity and magnetic performance of the iron oxide was improved (Fig. 7).[33,34]

3.5 The specific endocytosis of FA–PEG-*b*-PAA$_x$@SPION

The folate receptor expression of the RAW 264.7 cells could be largely up-regulated by the activation of IFN-γ/TNF-α.[17] The specificity targeting ability of FA–PEG-PAA@SPION to the folate receptor was tested through the Prussian blue staining of activated RAW 264.7 cells which have endocytosed PEG-*b*-PAA@SPIO or FA–PEG-*b*-PAA@SPIO. The conditions of the cellular endocytosis were optimized by changing the time and the concentration of the nanoparticles used (Fig. S4 and S5†). After that, the experiment was conducted to investigate the specific endocytosis of FA–PEG-*b*-PAA@SPION and PEG-*b*-PAA@SPION. Fig. 8 indicates that the cellular uptake amount of FA–PEG-*b*-PAA@SPION (blue granules) was more than that of PEG-*b*-

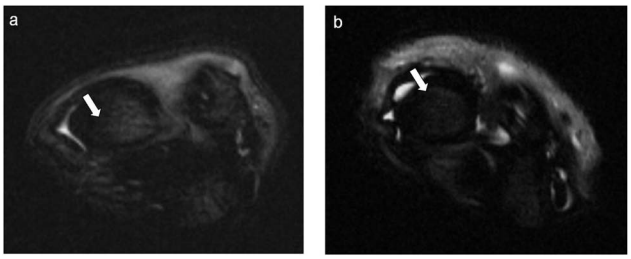

Fig. 9 PEG-*b*-PAA_{36}@SPION (a) and FA–PEG-*b*-PAA_{36}@SPION (b) contrast T_2 weighted MRI in the arthritic rat ankle joint 24 h after the intravenous injected of the SPIONs (the arrows indicate the synovium sites).

PAA@SPION, which proved the specific targeting ability of folic acid. Moreover, the amount of cellular uptake of FA–PEG-*b*-PAA_{36}@SPION was obviously larger than that of FA–PEG-*b*-PAA_{57}@SPION. The iron concentrations of the cellular uptake amount were measured by a ferrozine assay (Fig. S6†) and the results were consistent with the Prussia staining. The cellular uptake amounts of FA–PEG-*b*-PAA@SPION were two times larger than those of PEG-*b*-PAA@SPION, while the cellular uptake amount of FA–PEG-*b*-PAA_{36}@SPION was nearly four times larger than that of FA–PEG-*b*-PAA_{57}@SPION. These results indicated that FA–PEG-*b*-PAA_{36}@SPION was a preferable SPION for active targeting compared to FA–PEG-*b*-PAA_{57}@SPION.

3.6 The SPION enhanced MRI of antigen-induced arthritis

The AIA model was successfully built by the intradermal injection of complete Freund's adjuvant in the back feet of the rats. Inflammatory cells (arrow) like macrophages could be found in the synovium and the peripheral area of the arthritic joint in the light micrographs of the hematoxylin–eosin stain sample (Fig. S7†). Based on the magnetic properties test and endocytosis experiment, FA–PEG-*b*-PAA_{36}@SPION was chosen as the preferable nanoparticle for the MRI application of theRA joint. Representative T_2-weighted images of the SPION groups using 7T MRI equipment are presented in Fig. 9. The synovium of the animals appeared to have a moderate signal decline on the T_2-weighted MR images after intravenous injection of PEG-*b*-PAA_{36}@SPION (Fig. 9a). This finding indicated that the non-specific SPIONs could passively target the RA joint. In comparison, the FA–PEG-*b*-PAA_{36}@SPION contrasted MRI demonstrated a more intact and clearer structure of the synovium (Fig. 9b), suggesting that the SPIONs were preferentially endocytosed by macrophages in the inflamed synovium. For FA–PEG-*b*-PAA_{36}@SPION, the signal intensity ratio of the surrounding water proton/the arrowhead indicated area was 1.410 times larger than that of PEG-*b*-PAA_{36}@SPION, which indicated that the signal decrease of the arrow indicated area contrasted by FA–PEG-*b*-PAA_{36}@SPION was larger than that of PEG-*b*-PAA_{36}@SPION. These results suggested that the FA–PEG-*b*-PAA_{36}@SPION might be useful as a target MRI contrast to qualify the arthritic joint.

To better understand the targeting ability and biodistribution of the nanoparticles, the ankle joint and major organs including the liver, spleen, kidney, heart and lung were harvested and stained by Prussian blue after MRI (Fig. 10). The results indicated that PEG-*b*-PAA_{36}@SPION could passively accumulate in the ankle joint, whereas FA–PEG-*b*-PAA_{36}@SPION has shown a qualitative better accumulation in the joint, which might be due to the active targeting of folic acid. Except for the joint, the spleen and lung were found to have a small amount of SPION accumulation, which might be attributed to the macrophage endocytosis of the nanoparticles by reticulo-endothelial systems,[32,35] while the liver, heart and kidney showed little accumulation of the nanoparticle.

4 Conclusion

In summary, a novel PEG-*b*-PAA@SPION contrast agent was synthesized by using an *in situ* polyol method. Nanoparticles of

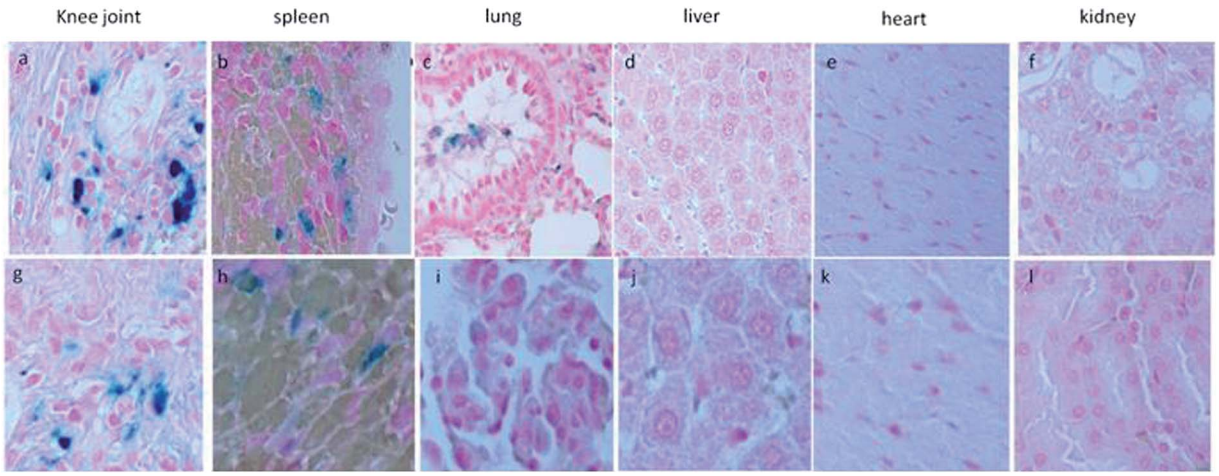

Fig. 10 Prussian blue staining images of the major organs including the ankle joint (a and g), spleen (b and h), lung (c and i), liver (d and j), heart (e and k) and kidney (f and l) one day after the injection of FA–PEG-*b*-PAA_{36}@SPION (a–f) and PEG-*b*-PAA_{36}@SPION (g–l) 24 h after the intravenous injected of SPION.

different sizes were obtained by controlling the chain length of the PAA block of the copolymer PEG-*b*-PAA_x. By measuring the magnetic sensitivity, colloid stability and specific targeting ability, FA–PEG-*b*-PAA_{36}@SPION was chosen as a contrast agent for the MRI of an RA joint. The signal of synovium was significantly enhanced in the 7T MRI after the administration of FA–PEG-*b*-PAA_{36}@SPION in AIA model rats. The correlated histological outcome of the Prussia blue staining also confirmed the excellent permeability efficiency of the folic acid conjugated PEG-*b*-PAA_{36}@SPION in the joint. The enhanced MR imaging results proved significant opportunity for the FA–PEG-PAA@SPION contrast agent for targeted human diagnosis of rheumatoid arthritis.

Acknowledgements

This work was financially supported by the National Natural Science Foundation of China (Grant no. 21304099, 51203162, 51103159, 51373177), the National High Technology Research and Development Program (Grant no. 2014AA020708, 2012AA022703 and 2012AA020804), Instrument Developing Project of the Chinese Academy of Sciences (Grant no. YZ201253, YZ201313), Open Funding Project of the National Key Laboratory of Biochemical Engineering (Grant no. Y22504A169). "Strategic Priority Research Program" of the Chinese Academy of Sciences, Grant no. XDA09030301-3.

References

1 H. K. Choi, M. A. Hernan, J. D. Seeger, J. M. Robins and F. Wolfe, *Lancet*, 2002, **359**, 1173–1177.
2 F. M. McQueen, *Rheumatology*, 2000, **39**, 700–706.
3 G. H. Simon, J. von Vopelius-Feldt, M. F. Wendland, Y. Fu, G. Piontek, J. Schlegel, M. H. Chen and H. E. Daldrup-Link, *J. Magn. Reson. Imaging*, 2006, **23**, 720–727.
4 C. S. Reiner, A. M. Lutz, F. Tschirch, J. M. Froehlich, S. Gaillard, B. Marincek and D. Weishaupt, *Eur. Radiol.*, 2009, **19**, 1715–1722.
5 N. Butoescu, C. A. Seemayer, M. Foti, O. Jordan and E. Doelker, *Biomaterials*, 2009, **30**, 1772–1780.
6 A. G. Roca, S. Veintemillas-Verdaguer, M. Port, C. Robic, C. J. Serna and M. P. Morales, *J. Phys. Chem. B*, 2009, **113**, 7033–7039.
7 S. Tong, S. Hou, B. Ren, Z. Zheng and G. Bao, *Nano Lett.*, 2011, **11**, 3720–3726.
8 B. J. Dardzinski, G. Boivin, J. Lewis and R. Hirsch, *Arthritis Rheum.*, 1999, **42**, 119.
9 S. H. Wang, X. Y. Shi, M. Van Antwerp, Z. Y. Cao, S. D. Swanson, X. D. Bi and J. R. Baker, *Adv. Funct. Mater.*, 2007, **17**, 3043–3050.
10 X. Y. Shi, S. H. Wang, S. D. Swanson, S. Ge, Z. Y. Cao, M. E. Van Antwerp, K. J. Landmark and J. R. Baker, *Adv. Mater.*, 2008, **20**, 1671–1678.
11 D. F. Liu, W. Wu, J. J. Ling, S. Wen, N. Gu and X. Z. Zhang, *Adv. Funct. Mater.*, 2011, **21**, 1498–1504.
12 Y. Zhang, N. Kohler and M. Q. Zhang, *Biomaterials*, 2002, **23**, 1553–1561.
13 J. C. Li, L. F. Zheng, H. D. Cai, W. J. Sun, M. W. Shen, G. X. Zhang and X. Y. Shi, *Biomaterials*, 2013, **34**, 8382–8392.
14 C. M. Paulos, M. J. Turk, G. J. Breur and P. S. Low, *Adv. Drug Delivery Rev.*, 2004, **56**, 1205–1217.
15 M. A. Guo, C. L. Que, C. H. Wang, X. Z. Liu, H. S. Yan and K. L. Liu, *Biomaterials*, 2011, **32**, 185–194.
16 F. Sonvico, S. Mornet, S. Vasseur, C. Dubernet, D. Jaillard, J. Degrouard, J. Hoebeke, E. Duguet, P. Colombo and P. Couvreur, *Bioconjugate Chem.*, 2005, **16**, 1181–1188.
17 F. Schmitt, L. Lagopoulos, P. Kauper, N. Rossi, N. Busso, J. Barge, G. Wagnieres, C. Laue, C. Wandrey and L. Juillerat-Jeanneret, *J. Controlled Release*, 2010, **144**, 242–250.
18 X. Cai, H. Zhou, Y. F. Wong, Y. Xie, Z. Q. Liu, Z. H. Jiang, Z. X. Bian, H. X. Xu and L. Liu, *Biochem. Biophys. Res. Commun.*, 2005, **337**, 586–594.
19 L. E. W. LaConte, N. Nitin, O. Zurkiya, D. Caruntu, C. J. O'Connor, X. Hu and G. Bao, *J. Magn. Reson. Imaging*, 2007, **26**, 1634–1641.
20 A. M. Mohs, Y. D. Zong, J. Y. Guo, D. L. Parker and Z. R. Lu, *Biomacromolecules*, 2005, **6**, 2305–2311.
21 H. F. Xu, F. H. Meng and Z. Y. Zhong, *J. Mater. Chem.*, 2009, **19**, 4183–4190.
22 Y. P. Wang, M. Zhang, C. Moers, S. L. Chen, H. P. Xu, Z. Q. Wang, X. Zhang and Z. B. Li, *Polymer*, 2009, **50**, 4821–4828.
23 K. Xu, Y. Wang, Y. X. Wang, T. Yu, L. J. An, C. Y. Pan and R. Bai, *Polymer*, 2006, **47**, 4480–4484.
24 B. L. Wang, R. J. Ma, G. Liu, X. J. Liu, Y. H. Gao, J. Y. Shen, Y. L. An and L. Q. Shi, *Macromol. Rapid Commun.*, 2010, **31**, 1628–1634.
25 C. M. Cheng, F. J. Xu and H. C. Gu, *New J. Chem.*, 2011, **35**, 1072–1079.
26 S. Lefevre, D. Ruimy, F. Jehl, A. Neuville, P. Robert, C. Sordet, M. Ehlinger, J. L. Dietemann and G. Bierry, *Radiology*, 2011, **258**, 722–728.
27 S. C. Wuang, K. G. Neoh, E. T. Kang, D. W. Pack and D. E. Leckband, *J. Mater. Chem.*, 2007, **17**, 3354–3362.
28 C. Huang, K. G. Neoh and E.-T. Kang, *Langmuir*, 2011, **28**, 563–571.
29 X. Y. Shi, T. P. Thomas, L. A. Myc, A. Kotlyar and J. R. Baker, *Phys. Chem. Chem. Phys.*, 2007, **9**, 5712–5720.
30 J. H. Maeng, D.-H. Lee, K. H. Jung, Y.-H. Bae, I.-S. Park, S. Jeong, Y.-S. Jeon, C.-K. Shim, W. Kim, J. Kim, J. Lee, Y.-M. Lee, J.-H. Kim, W.-H. Kim and S.-S. Hong, *Biomaterials*, 2010, **31**, 4995–5006.
31 S. Laurent, D. Forge, M. Port, A. Roch, C. Robic, L. Vander Elst and R. N. Muller, *Chem. Rev.*, 2008, **108**, 2064–2110.
32 E. D. Smolensky, H. Y. E. Park, Y. Zhou, G. A. Rolla, M. Marjanska, M. Botta and V. C. Pierre, *J. Mater. Chem. B*, 2013, **1**, 2818–2828.
33 M. V. Kovalenko, M. I. Bodnarchuk, R. T. Lechner, G. Hesser, F. Schaffler and W. Heiss, *J. Am. Chem. Soc.*, 2007, **129**, 6352–6353.
34 X. W. Teng and H. Yang, *J. Mater. Chem.*, 2004, **14**, 774–779.
35 Y. M. Liu, K. Yang, L. Cheng, J. Zhu, X. X. Ma, H. Xu, Y. G. Li, L. Guo, H. W. Gu and Z. Liu, *Nanomed.: Nanotechnol., Biol. Med.*, 2013, **9**, 1077–1088.

